

## Chapter 2

### Red Emitting Fluorenes as the Efficient Host Emitter for Non-Doped Red Organic Light-Emitting Diodes

#### 2-1 Introduction

Organic light-emitting diodes (OLEDs) are likely to play an increasingly competitive role in the flat-panel-display market since the efficient device was fabricated by Tang and VanSlyke.<sup>[1]</sup> Indispensable components of blue-, green-, and red-light-emitting materials have been developed for full-color displays. Red-light-emitting materials with high brightness and pure color fidelity are scarce compared with blue- and green-emitting. Whereas short wavelength light-emitting blue or green fluorescent materials are commonly used as host-emitter or dopant, red fluorescent materials are less flexible and mostly limited to the dopant usage in the fabrication of red OLEDs. This is because of the nature of red-light-emitting materials.<sup>[2]</sup>: (I) Molecules are usually flat with extended  $\pi$ -conjugation or donor-acceptor substituted  $\pi$ -conjugated molecules with the strong intermolecular dipole-dipole interactions or  $\pi$ - $\pi$  stacking, which leads to a high tendency of molecular aggregation, so-called concentration quenching.; (II) The small energy bandgap between the highest occupied molecular orbital (HOMO) and the lowest unoccupied molecular orbital (LUMO) of the red-light emitters, which generally results in efficient, non-radiative relaxation of the excited state.

Red fluorophores are usually flat molecules with extended  $\pi$ -conjugation or donor-acceptor substituted  $\pi$ -conjugated molecules with strong dipole, for examples the non-polar but extensively  $\pi$ -conjugated dye of TPP (5,10,15,20-teraphenylporphyrin)<sup>[3]</sup> and the fluorescent laser dyes of Nile Red<sup>[4]</sup> and DCM (4-(dicyanomethylene)-2-methyl-6-[4-(dimethylaminostyryl)-4*H*-pyran]).<sup>[5]</sup> Although high emission of Nile Red and DCM in solution was observed, these three red fluorophore are prone to aggregation and thus heavy

fluorescence quenching in solid state showed in **Figure 2-1**. The fluorescence of the solid samples of Nile Red and TPP is virtually invisible.

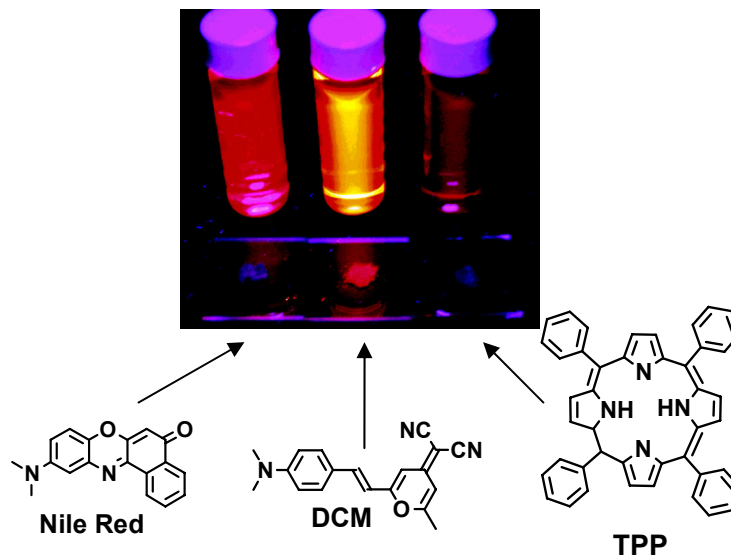


**Figure 2-1.** Fluorescence image of Nile Red, DCM and TPP in solution (1,4-dioxane) and in solid state.

Consequently, most red OLEDs take the guest-host doping system in order to prevent the molecular aggregation due to the intermolecular dipole-dipole interactions or  $\pi$ -stacking. The ideal doping level in the fabrication of dopant-based red OLED is often low ( $< 1\sim 2$  wt%) confining in a narrow doping range ( $\leq \pm 1$  wt%).<sup>[5]</sup> At low doping concentration, unsaturated red-light emission always occur due to the incomplete energy transfer from host to dopant or the insufficient carrier trapping of the dopant guest. At high doping concentration, concentration quenching lead to low electroluminescence (EL) quantum yield as well as red-shifting emission due to the solvatochromic polarization. In 1989, high photoluminescence (PL) quantum yield dye DCM was first adopted by Tang *et al.* in the investigation of the influence of device performance illustrate dopant approach. In **Figure 2-2**, the solid state fluorescence spectra of Alq<sub>3</sub> doped with DCM as a function of DCM concentration. The maxima relative fluorescence yield is 3.0% at the 0.5 mole% doping

concentration of DCM. The ideal doping concentration is between 0.25 mole% and 1 mole%, which is a relatively narrow range of doping concentration.<sup>[5]</sup>

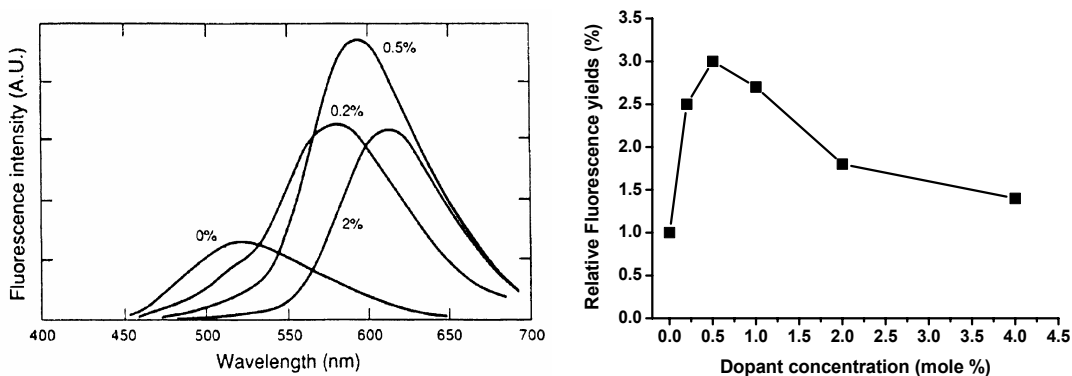


**Figure 2-2.** Fluorescence spectra of Alq<sub>3</sub> doped with DCM as a function of DCM concentration.<sup>[5]</sup>

In **Figure 2-3**, the devices showed high EL quantum efficiency (2.3%) at the optimum doping concentration which is about 0.1-0.5 mole% similar to the result of solid state photoluminescence (PL) studies. From a practical point of view, fabrication of dopant-based red OLEDs with such a low and narrow doping-concentration is not convenient for the rapid and mass production of OLEDs. Non-doped red OLEDs have attracted increasing interest because they are the alternative method to the current fabrication process of red OLEDs, which are nearly all fabricated by the less convenient doping process.

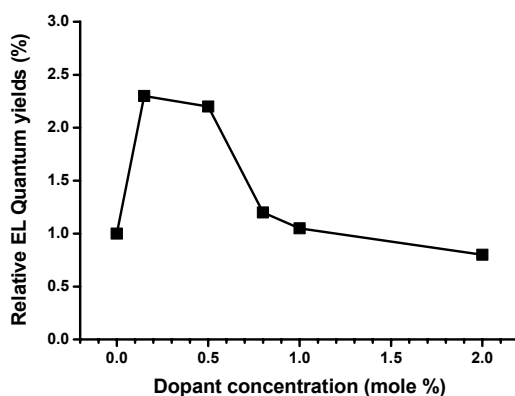


**Figure 2-3.** Relative EL quantum efficiencies as a function of dopant concentration in Alq<sub>3</sub> (ITO/diamine/Alq<sub>3</sub>:DCM/Mg:Ag).<sup>[5]</sup>

### 2-1-1 Recent non-doped red organic light-emitting diodes

In order to overcome these disadvantages, many research groups have tried to develop new amorphous host-emitting non-doped red fluorophores with saturated red luminescence instead of red fluorophores crystallized easily. In 2000, non-doped red host emitter **(PPA)(PSA)Pe-1** is a perylene-based fluorophore containing a styryl-appended diarylamine moiety showed in **Figure 3-4**.<sup>[6]</sup> Although the device showed red color chromaticity, CIE (Commission Internationale de l'Eclairage) coordinate,  $x = 0.64$ ,  $y = 0.35$ , its EL reached maximum luminance of  $4800 \text{ cd/m}^2$  at the driving voltage of 14 V. The device of **(PPA)(PSA)Pe-1** showed a short emission  $\lambda_{\text{max}}$  of 579 nm with a shoulder emission band  $\lambda_{\text{max}}$  of 620 nm that lead to the CIE coordinated in the satisfactory red region. The mission band  $\lambda_{\text{max}}$  of 620 nm was attributed to the excimer of the intermolecular coplanar  $\pi$ - $\pi$  interaction.

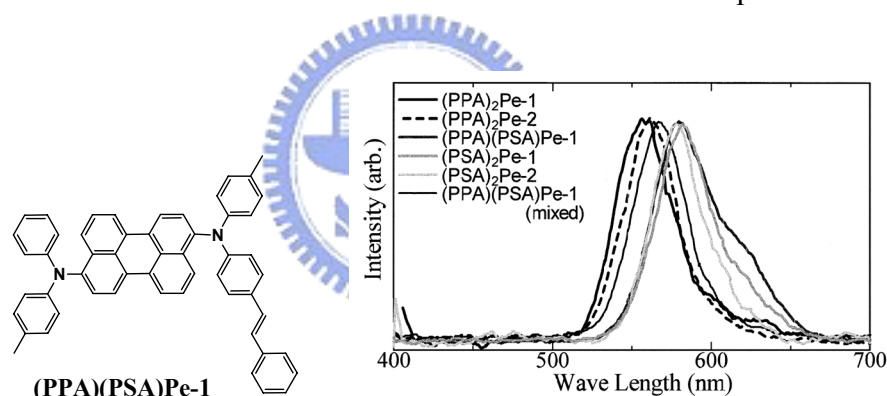


**Figure 2-4.** The chemical structure of **(PPA)(PSA)Pe-1**, and the EL spectra of devices.<sup>[6]</sup>

In 2003, the red host-emitting nondoped materials of **acen** were synthesized by Lin's group.<sup>[7]</sup> **(PPA)(PSA)Pe-1**, this series of **acen** compounds are also polycyclic aromatic hydrocarbon type species bearing diarylamine on benzo[*a*]aceanthrylene-cored subscript (**Figure 2-5**). These **acen** compounds were reported with glass transition temperature ( $T_g$ ) higher than 113 °C. Amorphous compounds of **acen3** and **acen4** showed high thermal stability than **acen1** by introducing the *tert*-butyl groups or the rigid anthranceyl groups to diarylamine segments. Pure red-emitting devices ( $\lambda_{\text{max}} = 622$ - $628 \text{ nm}$ , CIE coordinate  $x = 0.63$ - $0.66$ ,  $y = 0.32$ - $0.35$ ) generally can be achieved in a two-layer devices, three-layer

devices, or multilayered devices, ITO/**acen**/TPBI/Mg:Ag, ITO/NPB/**acen**/TPBI/Mg:Ag, ITO/NPB/**acen**/BCP/Alq<sub>3</sub>/Mg:Ag, respectively. In those devices, TPBI or Alq<sub>3</sub> was used as the electron-transporting layer BCP was used as hole-blocking layer (see **Figure 2-5**). The poor device performance ( $\eta_{\text{EXT}}^{\text{max}} < 0.68\%$ ) observed for those **acen** non-dopant OLEDs could be attributed to the low solution fluorescence quantum yield of **acen** compounds ( $\Phi_f = 5\text{-}12\%$ ).

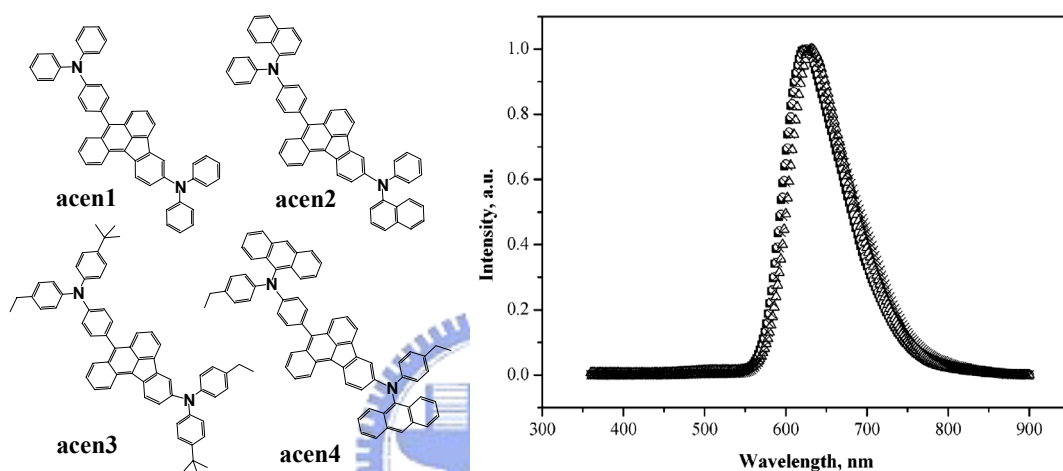


**Figure 2-5.** The chemical structures of **acn**, and the EL spectra of devices: ITO/NPB/**acn**/BCP/Alq<sub>3</sub>/Mg:Ag closed square: **acn1**, open circle: **acn2**, open triangle: **acn3**, cross: **acn4**.<sup>[7]</sup>

The donor-acceptor substituted  $\pi$ -conjugated molecules with strong dipole-dipole interaction in solid state always lead to fluorescence concentration quenching. However, molecules such as **BSN** (see **Figure 2-6**),<sup>[2c]</sup> **D-CN** (see **Figure 2-7**),<sup>[8]</sup> **btza** (see **Figure 2-8**),<sup>[9]</sup> and **NPAFN**<sup>[10]</sup> (see **Figure 2-9**) possess a pair of antiparallel dipoles, thus fluorescence concentration quenching in solid state due to dipole-dipole interaction can be substantially suppressed. Brightly red emitter (PL of  $\lambda_{\text{max}}$  at 630 nm with a quantum efficiency of 0.8) of 1,10-dicyano-substituted bis-styrylnaphthalene derivative **BSN** was developed by Sony in 2001. In a device of ITO/2-TNATA/NPB/**BSN**/Alq<sub>3</sub>/Li<sub>2</sub>O/Al, **BSN** was used as a non-dopant red emitter showing an impressive luminous efficiency of 2.8 cd/A at 500 cd/m<sup>2</sup>

with CIE coordinate,  $x = 0.63$ ,  $y = 0.37$ .<sup>[2c]</sup>

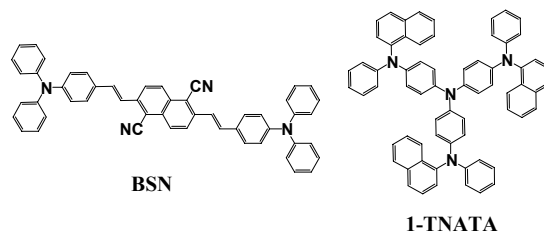


**Figure 2-6.** The chemical structures of **BSN** and 2-TNATA.

A similar red electroluminescent dye **D-CN** based on the bis(styryl) nucleus and synthesized by the bis-Knoevenagel condensation of 1,4- phenylenediacetonitrile and 2 eq. of 4-formyl-4-methoxytriphenylamine has also been reported in 2001. In **Figure 2-7**, device SL with a single-layer of ITO/**D-CN**/Mg:Ag was fabricated, and the maximum luminescence of 5080  $\text{cd}/\text{m}^2$  was achieved at 750  $\text{mA}/\text{cm}^2$ . In the case of double-layer device of ITO/**D-CN**/OXD/Mg:Ag, 3290  $\text{cd}/\text{m}^2$  of electroluminescence reveals in the 100  $\text{mA}/\text{cm}^2$  of current density. Both of these two devices emitted orange-red emission ( $\lambda_{\text{max}} \sim 597 \text{ nm}$ ) and showed high external quantum efficiency of 1.0% and 1.1%, respectively. It could be contributed to the dipolar characteristics of **D-CN**, such dipolar characteristic provides properties of charges injection and transportation. A better charge balance is expected to achieve with such materials. From molecular structure point of view, two CN groups work as electron injection and transport parts and two arylamino groups are capable of hole injection and transport.

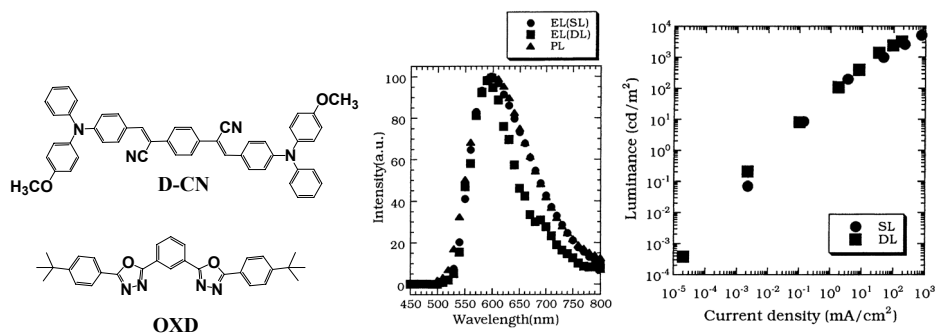


**Figure 2-7.** The chemical structures of **D-CN** and **OXD**, and the characterization of devices. (Closed circle: ITO/**D-CN**/Mg:Ag; closed square: ITO/**D-CN**/OXD/Mg:Ag).<sup>[8]</sup>

Another series of bipolar compounds containing a benzo[1,2,5]thiadiazole core and peripheral diarylamines and/or 4-tert-butylphenyl moieties have been developed by Lin et al in 2004 (Figure 2-8). The higher  $T_g$  (**btza1**: 97 °C, **btza2**: 112 °C, **btza3**: 117 °C) of these compounds were associated with a lower tendency of crystallization and great stability of the amorphous glass state by introducing peripheral diarylamines moieties. Except **btza1**, two types red host-emitting nondoped devices ITO/**btza**/TPBI/Mg:Ag and ITO/**btza**/Mg:Ag are fabricated. The best performance of ITO/**btza3**/TPBI/Mg:Ag device exhibited maximum EL intensity of 9138 cd/m<sup>2</sup> with CIE coordinate,  $x = 0.63$ ,  $y = 0.35$ , and maximum external quantum efficiency of 1.7%.

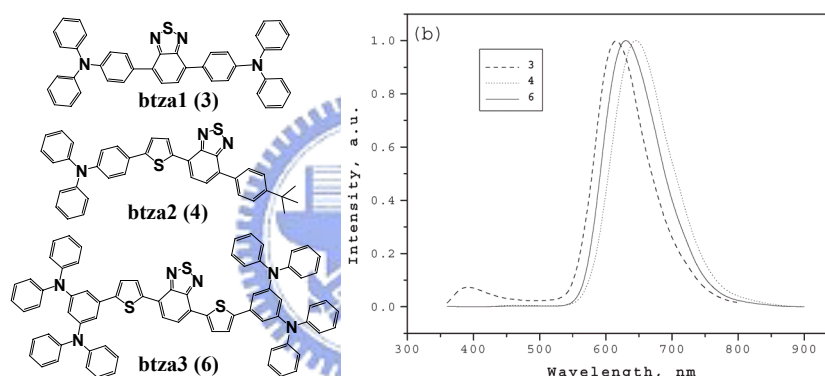


**Figure 2-8.** The chemical structures **btza1**, **btza2** and **btza3**, and electroluminescence spectra of ITO/**btza**/TPBI/Mg:Ag.<sup>[9]</sup>

Red fluorophore **NPAFN** is suitable for high performance non-doped red OLEDs, because of the high thermal stability ( $T_g \sim 109$  °C,  $T_m \sim 260$  °C, no sign of crystallization) and brightly fluorescent in the solid state. Significantly, **NPAFN** can be easily prepared in a simple two-step procedure (see **Figure 2-9**) with overall isolated yield > 45%. **NPAFN** is unusual because it is brightly fluorescent but only in the solid state not in solution. The poor fluorescence in solution may be due to the easily exchangeable multiple conformations of the nonplanar benzene and naphthalene rings of the molecule and the twin dipolar nature also contributes to the non-radiative relaxation of **NPAFN** in the excited state. The bulky and nonplanar arylamino substituents as well as fumaronitrile moiety were believed to play an

important role in preventing **NPAFN** from fluorescence quenching in solid state.

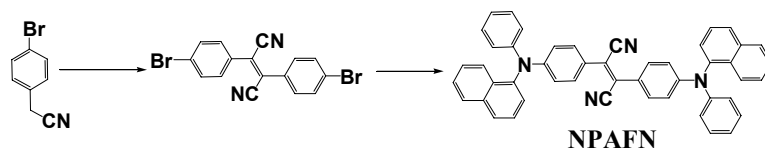


**Figure 2-9.** The synthetic route of **NPAFN**.<sup>[10]</sup>

Two OLED devices with configurations ITO/NPB/**NPAFN**/BCP/TPBI/Mg:Ag and ITO/**NPAFN**/BCP/TPBI/Mg:Ag were fabricated by Chen et al. The EL of the devices had emission maxima ( $\lambda_{\max}^{\text{el}}$ ) around 634 and 636 nm with the same CIE coordinate,  $x = 0.64$ ,  $y = 0.33$  (see **Figure 2-10**), although the spectra were broadened and red shifted (+18-20 nm) compared with the PL of the solid film. Usually, such a difference between PL and EL indicates there is a certain degree of aggregation formation of **NPAFN** providing charge-trapped sites with lower energy. The maximum intensity of EL reached 10034  $\text{cd}/\text{m}^2$  and 9359  $\text{cd}/\text{m}^2$  for the devices and the maximum quantum yield of devices reached 1.8% and 2.4% with and without NPB, respectively. Practically, at low current density of 20  $\text{mA}/\text{cm}^2$ , the device without NPB of **NPAFN** showed remarkable EL intensity of 455  $\text{cd}/\text{m}^2$  (see **Figure 2-10**), which was sufficiently bright for flat panel display application.

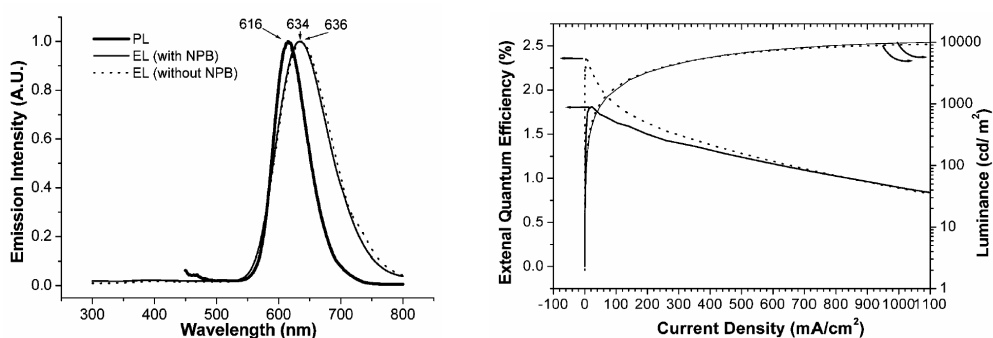


**Figure 2-10.** The PL and EL spectra of **NPAFN**; External quantum efficiency-Current Density-Luminance ( $\eta_{\text{EXT}}-I-L$ ); solid line: ITO/NPB/**NPAFN**/BCP/TPBI/MgAg and dotted line: ITO/**NPAFN**/BCP/TPBI/MgAg.<sup>[10]</sup>



The third type of nondoping red fluorescent material is similar to the second one but different in the alignment of the intramolecular dipoles. For examples, a series of thieno[3,4-*b*]pyrazine incorporated triarylamine in pyrazine ring and *tert*-butyl-phenyl groups in thiophene (see **Figure 3-11**).<sup>[11]</sup> This series of **TPZ** adopt a pair of vicinal triarylamine substituent as the electron-donor and a heterocyclic thienopyrazine as the electron-acceptor. Poor efficiency of the device ITO/**TPZ2**/TPBI/Mg:Ag showed maximum brightness of 1766 cd/m<sup>2</sup> with saturated red emission (CIE coordinate, x = 0.65, y = 0.33) and the maximum quantum yield of 0.5%. It was apparent that the poor device performance of **TPZ2** could not be the candidate of material for flat panel display application.

As similar to **TPZ** series, cyano groups were adopted as the electro-withdrawing moiety and triarylamine substituents as the electron-donor into **CAPP** and **CAPQ** (see **Figure 3-11**).<sup>[12]</sup> Good thermal stability of **CAPP** ( $T_g \sim 140$  °C,  $T_d \sim 458$  °C) and **CAPQ** ( $T_g \sim 245$  °C,  $T_d \sim 530$  °C) should be beneficial for devices prepared by vacuum deposition. Although the non-planarity and bulky structure can efficiency diminish the intermolecular  $\pi$ - $\pi$  stacking and thus concentration quenching in the solid state, only 0.7% of the maximum external quantum yield was obtained by the device of ITO/**CAPP**/BCP/Alq<sub>3</sub>/LiF/Al. **CAPP** and **CAPQ** were weak red emitters with maximum EL intensity of only 536 cd/m<sup>2</sup> (CIE coordinate, x = 0.65, y = 0.34) and 110 cd/m<sup>2</sup> (CIE coordinate, x = 0.67, y = 0.33), respectively.

**QPMA** was dibenzosuberene (DBE) templated with fused quinoxaline backbones of electronic attributes for optoelectronic applications.<sup>[13]</sup> **QPMA** connects the individual ortho-position of two phenyl rings in a HT-type 9,9-diphenylfluorene framework to the C2-C3 edge of a functionalized ET-type quinoxaline (see **Figure 3-11**). High thermal stability **QPMA** ( $T_g \sim 153$  °C,  $T_d \sim 333$  °C) was fabricated with the device of ITO/**QPMA**/BCP/Alq<sub>3</sub>/LiF/Al. It showed the highly bright and efficient red EL (644 nm) up to 11484 cd/m<sup>2</sup> at 14 V with external quantum efficiency as high as 3.17%.

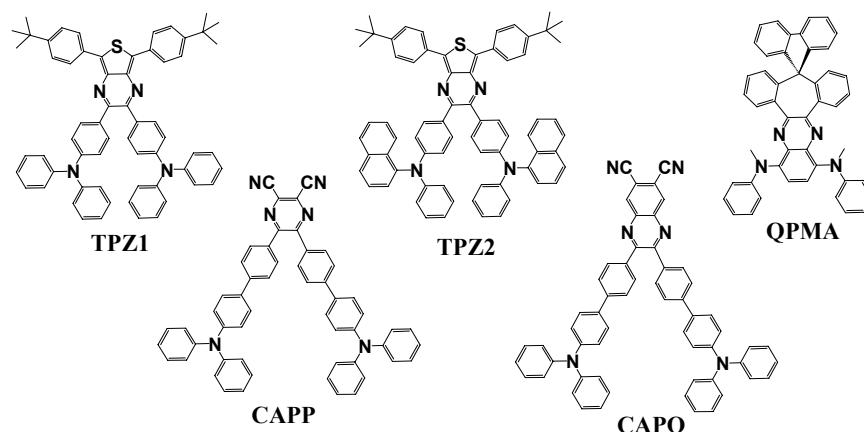


**Figure 2-11.** The chemical structures **TPZ1**, **TPZ2**, **CAPP**, **CAPQ** and **QPMA**.<sup>[11, 12, 13]</sup>

Furthermore, two symmetrical 3,4-substituted maleimides of **NPAMLMe**<sup>[14]</sup> and **INDMLMe**<sup>[15]</sup> were also adopted for host-emitting nondoped OLEDs (see **Figure 3-12**). **NPAMLMe** film was reported to be a truly amorphous molecular material by showing no detectable melting or crystallization signal but only glass transition temperature signals ( $T_g \sim 120$  °C) in all thermalgrams of DSC. The amorphous glassy of **NPAMLMe** thin film provide a good opportunity for the fabrication of nondoped device. A trilayer device ITO/**NPAMLMe**/BCP/TPBI/Mg:Ag was fabricated and showed red emission maximum of 650 nm with the satisfied red CIE coordinate  $x = 0.66$ ,  $y = 0.32$ . The brightness and efficient device of **NPAMLMe** showed near  $8000 \text{ cd/m}^2$  at 15 V and maximum external quantum efficiency of 2.4% (see **Figure 3-13**). Compared with **NPAMLMe**, the device performance of **INDMLMe** is inferior. Typical devices configured was ITO/NPB/**INDMLMe**/TPBI/Mg:Ag and showed maximum brightness of  $1750 \text{ cd/m}^2$  at about 13 V and external quantum efficiency of 0.5%.

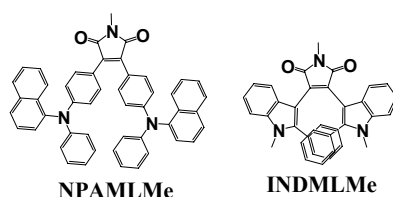


**Figure 2-12.** The chemical structures **NPAMLMe** and **INDMLMe**.<sup>[14,15]</sup>

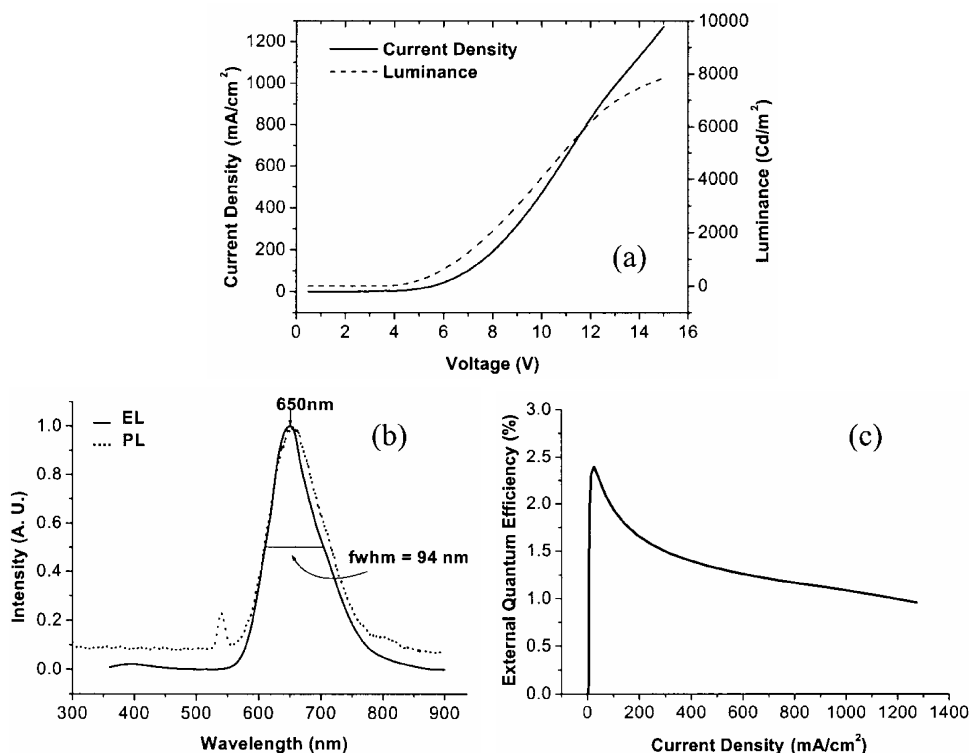


**Figure 2-13.** The PL and EL spectra of NPAMLMe; (a) Current Density-Voltage-Luminance ( $I$ - $V$ - $L$ ), (b) PL of solid film and EL spectra, (c) External quantum efficiency-Current Density ( $\eta_{EXT}$ - $I$ ).<sup>[14]</sup>

The data of the EL performance of non-doped host-emitting red OLEDs were collected in **Table 2-1**. NPAMLMe, NPAFN, QPMA and batz3 are currently the most satisfactory materials for practical application. The current performance of nondoped red OLEDs still falls behind that of dopant-based red OLEDs, but the lagging distance is closing up as their evolution progresses. Up to now, there are very few non-dopant red materials suitable for the display application because of the insufficient efficiency of devices. Not only the efficiency but also the thermal stability are still remained to be improved for non-dopant red materials.

**Table 2-1.** The EL Performance of Non-Doped Host-Emitting Red OLEDs recently.

Material	$\lambda_{\max}^{\text{el}}$ (nm)	CIE (x, y)	Max. luminance, at 100 mA/cm <sup>2</sup> , at 20 mA/cm <sup>2</sup> (cd/m <sup>2</sup> )	Max. efficiency (%, cd/A, lm/W)	Ref.
<b>(PPA)(PSA)Pe-1<sup>a</sup></b>	579	0.64, 0.35	4800, -, -	-, 1.1, -	6
<b>acen1<sup>b</sup></b>	626	0.65, 0.35	4514, 516, -	0.49, 0.52, 0.23	7
<b>acen2<sup>b</sup></b>	624	0.65, 0.35	4643, 604, -	0.68, 0.77, 0.60	7
<b>acen3<sup>b</sup></b>	630	0.65, 0.34	2705, 299, -	0.33, 0.31, 0.27	7
<b>acen4<sup>b</sup></b>	626	0.66, 0.34	1764, 350, -	0.37, 0.36, 0.17	7
<b>BSN<sup>c</sup></b>	630	0.63, 0.37	-, -, -	-, 2.8, -	2c
<b>D-CN<sup>d</sup></b>	597	-, -	5080, 1440, 600	1, -, -	8
<b>D-CN<sup>e</sup></b>	598	-, -	3500, 3290, 700	1.1, -, -	8
<b>btza3<sup>f</sup></b>	626	0.65, 0.35	9138, 1415, -	1.7, 2.0, 1.6	9
<b>btza3<sup>g</sup></b>	626	0.64, 0.36	7952, 597, -	0.51, 0.60, 0.44	9
<b>NPAFN<sup>h</sup></b>	636	0.64, 0.33	9359, 1800, 455	2.4, 2.5, 1.7	10
<b>NPAFN<sup>i</sup></b>	634	0.64, 0.33	10034, 1700, 392	1.8, 2.0, 0.9	10
<b>TPZ1<sup>j</sup></b>	-	0.65, 0.33	1766, 324, 69	0.5, 0.34, 0.17	11
<b>TPZ2<sup>k</sup></b>	-	0.59, 0.33	3834, 556, 131	0.84, 0.65, 0.40	11
<b>CAPP<sup>l</sup></b>	631	0.65, 0.34	536, -, -	0.70, -, -	12
<b>CAPQ<sup>m</sup></b>	657	0.67, 0.33	110, -, -	0.18, -, -	12
<b>QPMA<sup>n</sup></b>	644	-, -	11484, -, 1102	3.17, 2.31, 1.21	13
<b>NPAMLM<sup>o</sup></b>	650	0.66, 0.32	8000, 1260, 300	2.4, 1.5, 0.9	14
<b>INDMLM<sup>p</sup></b>	650	0.63, 0.36	1750, -, -	0.54, -, -	15

<sup>a</sup>ITO/starburst amine/(PPA)(PSA)Pe-1/quinoline metal complex/Mg:Ag; <sup>b</sup>ITO/NPB/acen/BCP/Alq<sub>3</sub>/Mg:Ag; <sup>c</sup>ITO/2-TNATA/NPB/BSN/Alq<sub>3</sub>/Li<sub>2</sub>O/Al; <sup>d</sup>ITO/D-CN/Mg:Ag; <sup>e</sup>ITO/D-CN/OXD/Mg:Ag; <sup>f</sup>ITO/btaz3/TPBI/Mg:Ag; <sup>g</sup>ITO/btaz3/Mg:Ag; <sup>h</sup>ITO/NPAFN/BCP/TPBI/Mg:Ag; <sup>i</sup>ITO/NPB/NPAFN/BCP/TPBI/Mg:Ag; <sup>j</sup>ITO/TPZ1/TPBI/Mg:Ag; <sup>k</sup>ITO/TPZ2/TPBI/Mg:Ag; <sup>l</sup>ITO/CAPP/BCP/Alq<sub>3</sub>/LiF/Al; <sup>m</sup>ITO/CAPQ/BCP/Alq<sub>3</sub>/LiF/Al; <sup>n</sup>ITO/QPMA/BCP/Alq<sub>3</sub>/LiF/Al; <sup>o</sup>ITO/NPAMLM/BCP/TPBI/Mg:Ag; <sup>p</sup>ITO/NPB/INDMLM/TPBI/Mg:Ag.

## 2-2 Motivation of research

Although a wide range of donor-acceptor-substituted fluorene derivatives are known,<sup>[16]</sup> none of them shows long wavelength red fluorescence ( $\lambda_{\max}^{\text{fl}} > 620$  nm). As **Figure 2-14** showed, from a molecular design point of view, it is easy to functionalize on the 2- and 7-positions of fluorene moiety in deriving various fluorophores. On the other hand, functionalization at the 9,9'-position of fluorene offers the possibility of controlling molecular

interaction in solid state. Besides, the orthogonal 9,9'-spirobifluorene rigid structure seems attractive for preventing molecules from  $\pi$ - $\pi$  stacking. It has been demonstrated by Salbeck et al. for preventing the close packing of molecules and generating amorphous glass materials with morphological stability.<sup>[17]</sup>

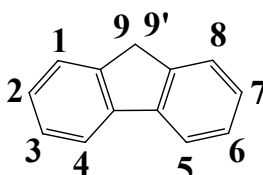


**Figure 2-14.** The chemical structure of fluorene.

In the development of red fluorophores for OLEDs, recently we and others have reported efficient host emitting, non-doped, red OLEDs.<sup>[2c, 6-15]</sup> Particularly, red fluorophores based on arylamino-substituted diphenylmaleimide<sup>[14]</sup> or diphenylfumaronitrile<sup>[10]</sup> have limited fluorescence quenching in solid state and the substituent of arylamino group is one of determining factor. Arylamino moieties are nonplanar and well known for their morphological characteristics in forming amorphous molecular glasses.<sup>[18]</sup> Dicyanovinyl moieties were a well-known in common used for optical electronic and nonlinear optical compounds due to the strong electron accepting property. Laser dye of 2-(4-diphenylamino-benzylidene)-malononitrile had been used as a dopant in PVK for electroluminescence device in 1997.<sup>[19]</sup> Herein we designed a new type of red emitter for non-doped red OLEDs based on donor-acceptor-substituted fluorenes. Such donor (arylamino) and acceptor (dicyanovinyl) will provide the right combination in tuning the emission color to red region. In order to prevent the fluorescence concentration quenching in solid state, we take the advantage of arylamino as well as the spiro-annulated structures for red emitting fluorene fluorophores.

## 2-3 Experimental

### 2-3-1 Materials

2,7-Dibromo-9,9'-dipropylfluorene<sup>[20]</sup> and 2,7-dibromo-9,9-spirobifluorene<sup>[21]</sup> were synthesized according to literature procedures. Diphenylamine, di-*p*-tolylamine (97%), palladium(II) acetate (Pd(OAc)<sub>2</sub>) with 47.5% palladium, tri-*tert*-butylphosphine 99% (P(<sup>*t*</sup>Bu)<sub>3</sub>), cesium carbonate (Cs<sub>2</sub>CO<sub>3</sub>), malononitrile, basic aluminum oxide (Al<sub>2</sub>O<sub>3</sub>), *n*-butyllithium (*n*-BuLi) 1.6 M in hexane, *N,N'*-dimethylformamide (DMF), tetrahydrofuran (THF), calcium hydride, benzophenone, toluene, dichloromethane, ethyl acetate and hexane were purchased from Acros, Fluka, Aldrich, Riedel-dehaën, TCI, Merck or Mallunckrodt. DMF was distilled by calcium sulfate under reduced pressure. Toluene was distilled under nitrogen from calcium hydride. THF was distilled under nitrogen from sodium benzophenone ketyl, and the other solvents of were dried using standard procedures. All other reagents were used as received from commercial sources unless otherwise stated.

### 2-3-2 Instruments

<sup>1</sup>H and <sup>13</sup>C NMR spectra were recorded on a Bruker AMX-400 MHz, AV-400 MHz and AV-500 MHz Fourier transform spectrometer at room temperature. Elemental analyses were recorded by a Perkin-Elmer 2400 CHN Elemental Analyzer. Mass Spectroscopic of compounds was recorded by the Mass Spectroscopic Laboratory in-house service of the Institute of Chemistry, Academia Sinica that using Fast Atom Bombardment (FAB) type or Electron Impact Ionization (EI) of mass spectra (on a VG Analytical 11-250J). Photoluminescence (PL) spectra were recorded on a Hitachi fluorescence spectrophotometer F-4500. The Absorption spectra were recorded by a UV-visible absorption spectrophotometer Hewlett-Pacher 8453. Melting points (*T*<sub>m</sub>), glass transition temperatures (*T*<sub>g</sub>), and crystallization temperatures (*T*<sub>c</sub>) of respective compound were measured by differential

scanning calorimetry (DSC) using a Perkin-Elmer DSC-6 differential scanning calorimeter. Thermogravimetric analysis (TGA) using a Perkin-Elmer DSC-7 thermogravimetric analyzer was used to determine the decomposition temperatures ( $T_d$ ) of the compounds. The onset of the weight loss immediately was defined as  $T_d$ . Both thermal analysis methods were performed under nitrogen atmosphere with scanning (both heating and cooling) rate of 10 °C/min. The ionization potentials (or HOMO energy levels) of fluorene derivative compounds were determined by low energy photo-electron spectrometer (Riken-Keiki AC-2). LUMO energy levels were estimated by subtracting the energy gap ( $\Delta E$ ) from HOMO energy levels.  $\Delta E$  was determined by the onset absorption energy from absorption spectra of the materials.

The quantum yields of emitting fluorophores were determined by integrating-sphere method described by de Mello et al. on vacuum deposited thin films.<sup>[16]</sup> HeCd laser beam (325 or 442 nm) interacts with a liquid or solid sample located inside an integrating sphere with internal diffuse white reflectance coating. Through a baffle-blocked opening, the uniformly scattered radiation is coupled to a fused-silica fiber and is detected by a spectrally-calibrated spectrometer-CCD system. We estimate the error of  $\Phi_f$  by repeated measurements on several dyes with known  $\Phi_f$  values. Nile Red (in 1,4-dioxane) was one of the fluorescent dyes and the corresponding  $\Phi_f$  was determined as  $67 \pm 5\%$ , which was quite close to the literature value of  $68\%$ .<sup>[4]</sup>

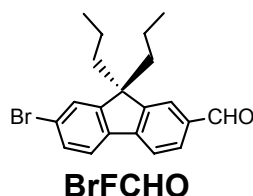
Single crystals of samples suitable for x-ray diffraction were grown by slow evaporation of hexane solution containing the compound. Data collection was carried out on a Bruker X8APEX CCD diffractometer at room temperature or 100 K, respectively. The radiation of Mo radiation ( $\lambda = 0.71073 \text{ \AA}$ ) was used for both crystals. The unit cell parameters were obtained by a least-square fit to the automatically centered settings for reflections. Intensity data were collected by using  $\omega/2\theta$  scan mode. Corrections were made for Lorentz and polarization effects. The structures were solved by direct methods *SHELX-97*.<sup>[22]</sup> All non-hydrogen atoms were located from the difference Fourier maps and were refined by

full-matrix least-squares procedures. Hydrogen atoms were calculated and refined with an overall isotropic temperature factor. Calculations and full-matrix least-squares refinements were performed utilizing the *WINGX* program package<sup>[23]</sup> in the evaluation of values of  $R(F_o)$  for reflections with  $I > 2\sigma(I)$  and  $R_w(F_o)$ , where  $R = \Sigma||F_o| - |F_c||/\Sigma|F_o|$  and  $R_w = [\Sigma\{w(F_o^2 - F_c^2)^2\}/\Sigma\{w(F_o^2)^2\}]^{1/2}$ .

Materials NPB, BCP, and Alq<sub>3</sub> are 1,4-bis(1-naphthylphenylamino)biphenyl, 2,9-dimethyl-4,7-diphenyl-1,10-phenanthroline and tris(8-hydroxyquinoline)aluminum, respectively. Fabrication of OLEDs was conducted by high-vacuum (10<sup>-6</sup> torr) thermal evaporation of the material onto pre-cleaned indium-tin-oxide (ITO)-coated glass (Merck Display Technology, Taiwan) with a sheet resistance < 50 Ω/sq. The pre-treatment of ITO includes a routine chemical cleaning using detergent and alcohol in sequence, followed by oxygen plasma cleaning. The measurements for devices were made at room temperature under ambient conditions. The EL spectra were measured using the fluorescence spectrophotometer by blocking the incident light. EL characterization, including luminance (cd/m<sup>2</sup>), current density (mA/cm<sup>2</sup>), driving voltage (V), and external quantum efficiency (%), have been described before.<sup>[24]</sup>

### 2-3-3 Synthesis

#### Synthesis of 7-bromo-9,9'-dipropyl-9H-fluorene-2-carboxaldehyde (BrFCHO)



To a THF solution (200 mL) containing 2,7-dibromo-9,9'-dipropylfluorene (14 g, 34.3 mmol) was added *n*-BuLi (24 mL, 37.7 mmol, 1.6 M in hexane) slowly at -78 °C. The mixture was stirred for 2 h under nitrogen atmosphere. After the slow addition of DMF (10



mL), the reaction solution was kept at  $-78\text{ }^{\circ}\text{C}$  for 1 h. The reaction mixture was then warmed to room temperature and stirred overnight. Saturated ammonium chloride solution was added to the reaction solution. The solution was extracted with ethyl acetate, dried over  $\text{MgSO}_4$ , and concentrated under reduced pressure. The residual solid was subjected to flash column chromatography (silica gel, dichloromethane/hexanes: 1/20) to give a white solid. Yield: 81.6% (10.1 g).  $^1\text{H}$  NMR (400 MHz,  $\text{CDCl}_3$ ):  $\delta$  [ppm] 10.04 (s, 1H), 7.85 (s, 1H,  $J = 1.3$  Hz), 7.84 (dd, 1H,  $J = 7.7$  Hz, 1.3 Hz), 7.78 (d, 1H,  $J = 7.7$  Hz), 7.61 (d, 1H,  $J = 8.0$  Hz), 7.51 (d, 1H,  $J = 1.6$  Hz), 7.49 (dd, 1H,  $J = 8.0$  Hz, 1.6 Hz), 2.01-1.92 (m, 4H), 0.68-0.55 (m, 10H).  $^{13}\text{C}$  NMR (100 MHz,  $\text{CDCl}_3$ ):  $\delta$  [ppm] 192.1, 154.2, 151.1, 146.3, 128.5, 135.6, 130.5, 130.4, 126.5, 123.1(x2), 122.2, 120.0, 55.8, 42.3, 17.1, 14.2. FAB-MS: calcd. MW, 356.1,  $m/e = 357.1/359.1$  ( $\text{M}+\text{H}$ ) $^+$ .

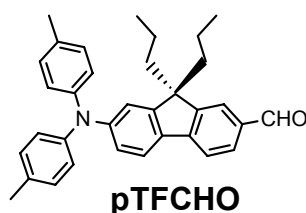
### Synthesis of 7-bromo-9,9'-spirobifluorene-2-carboxaldehyde (BrSPCHO)



To a THF solution (350 mL) containing 2,7-dibromo-9,9'-spirobifluorene (7 g, 14.8 mmol) was added *n*-BuLi (9.3 mL, 14.8 mmol, 1.6 M in hexane) slowly at  $-78\text{ }^{\circ}\text{C}$ . The mixture was stirred for 2 h under nitrogen atmosphere. After the slow addition of DMF (5 mL), the reaction solution was kept at  $-78\text{ }^{\circ}\text{C}$  for 1 h. The reaction mixture was then warmed to room temperature and stirred overnight. Saturated ammonium chloride solution was added to the reaction solution. The solution was extracted with ethyl acetate, dried over  $\text{MgSO}_4$ , and concentrated under reduced pressure. The residue solid was subjected to flash column chromatography (silica gel, dichloromethane/hexanes: 1/10) to give white solid. Yield: 75% (4.7 g).  $^1\text{H}$  NMR (400 MHz,  $\text{CDCl}_3$ ):  $\delta$  [ppm] 9.82 (s, 1H), 7.95 (d, 1H,  $J = 7.8$  Hz), 7.91 (dd, 1H,  $J = 7.9$  Hz, 1.4 Hz), 7.87 (d, 2H,  $J = 8.4$  Hz), 7.78 (d, 1H,  $J = 8.2$  Hz), 7.54

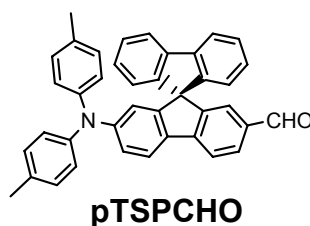
(dd, 1H,  $J = 8.2$  Hz, 1.8 Hz), 7.41 (td, 2H,  $J = 7.5$  Hz, 1.0 Hz), 7.23 (s, 1H,  $J = 1.4$  Hz), 7.13 (td, 2H,  $J = 7.5$  Hz, 1.0 Hz), 6.91 (d, 1H,  $J = 1.8$  Hz), 7.87 (d, 2H,  $J = 8.2$  Hz).  $^{13}\text{C}$  NMR (100 MHz,  $\text{CDCl}_3$ ):  $\delta$  [ppm] 191.4, 152.1, 149.5, 146.7, 146.6, 141.8, 139.1, 136.3, 131.4, 130.3, 128.4, 128.1, 127.6, 125.3, 123.9, 123.4, 122.4, 120.4, 120.4, 65.6. FAB-MS: calcd. MW, 422.0,  $m/e = 423.1/425.1$  ( $\text{M}+\text{H}$ ) $^+$ .

### Synthesis of 7-(di-*p*-tolylamino)-9,9'-dipropyl-9H-fluorene-2-carboxaldehyde (pTFCHO)



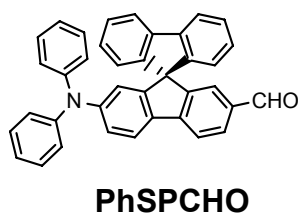
Under nitrogen atmosphere, a mixture of 7-bromo-9,9'-dipropylfluorene-2-carboxaldehyde (5 g, 13.99 mmol), di-*p*-tolylamine (4.14 g, 20.99 mmol),  $\text{Pd}(\text{OAc})_2$  (0.078 g, 0.35 mmol, 2.5 mol%),  $\text{P}(\text{tBu})_3$  (0.142 g, 0.7 mmol, 5 mol%), and  $\text{Cs}_2\text{CO}_3$  (10.25 g, 31.5 mmol) in toluene (25 mL) was heated at 120 °C with stirring overnight. After cooling to room temperature, saturated ammonium chloride solution was added to the reaction solution. The solution was extracted with ethyl acetate, dried over  $\text{MgSO}_4$ . The solution was concentrated under reduced pressure and subjected to flash column chromatography (silica gel, dichloromethane/hexanes: 1/2). A greenish yellow solid was obtained. Yield: 86% (5.7g).  $^1\text{H}$  NMR (400 MHz,  $\text{CDCl}_3$ ):  $\delta$  [ppm] 9.99 (s, 1H), 7.79 (s, 1H,  $J = 1.4$  Hz), 7.78 (dd, 1H,  $J = 7.7$  Hz, 1.4 Hz), 7.66 (d, 1H,  $J = 7.7$  Hz), 7.53 (d, 1H,  $J = 8.3$  Hz), 7.08-7.04 (m, 5H), 7.01 (d, 4H, 8.5 Hz), 6.94 (dd, 1H,  $J = 8.3$  Hz, 2.1 Hz), 2.32 (s, 6H), 1.94-1.75 (m, 4H), 0.71-0.58 (m, 10H).  $^{13}\text{C}$  NMR (100 MHz,  $\text{CDCl}_3$ ):  $\delta$  [ppm] 192.2, 153.6, 151.1, 149.3, 147.8, 145.2, 134.2, 133.0, 132.9, 130.9, 129.9, 124.7, 122.7, 121.5(x2), 118.9, 116.8, 55.2, 42.4, 20.8, 17.2, 14.4. FAB-MS: calcd. MW, 473.7,  $m/e = 473.3$  ( $\text{M}^+$ ).

### Synthesis of 7-(di-*p*-tolylamino)-9,9'-spirobifluorene-2-carboxaldehyde (pTSPCHO)



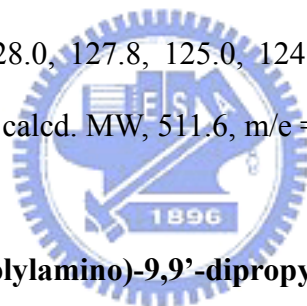
Under nitrogen atmosphere, a mixture of 7-bromo-9,9'-spirobifluorene-2-carboxaldehyde (3.2 g, 7.8 mmol), di-*p*-tolylamine (2.3 g, 11.7 mmol), (0.044 g, 0.20 mmol, 2.5 mol%), P(<sup>t</sup>Bu)<sub>3</sub> (0.08 g, 0.40 mmol, 5 mol%), and Cs<sub>2</sub>CO<sub>3</sub> (5.72 g, 17.55 mmol) in toluene (16 mL) was heated at 90 °C with stirring overnight. After cooling to room temperature, saturated ammonium chloride solution was added to the reaction solution. The solution was extracted with ethyl acetate, dried over MgSO<sub>4</sub>. The solution was concentrated under reduced pressure and subjected to flash column chromatography (silica gel, ethyl acetate/hexanes: 1/5). A greenish yellow solid was obtained. Yield: 75% (3.5g). <sup>1</sup>H NMR (400 MHz, CDCl<sub>3</sub>): δ [ppm] 9.74 (s, 1H), 7.83 (dd, 1H, *J* = 8.0 Hz, 1.4 Hz), 7.79 (d, 1H, *J* = 7.8 Hz), 7.76 (d, 2H, *J* = 7.6 Hz), 7.66 (d, 1H, *J* = 8.4 Hz), 7.33(td, 2H, *J* = 7.6 Hz, 1.0 Hz), 7.14–7.09 (m, 3H), 6.95–6.90 (m, 5H), 6.82 (d, 4H, 8.4 Hz), 6.76 (d, 2H, 7.6 Hz), 6.52 (d, 1H, 2.1Hz), 2.23 (s, 6H). <sup>13</sup>C NMR (100 MHz, CDCl<sub>3</sub>): δ [ppm] 191.6, 151.4, 149.6(x2), 148.0, 147.7, 144.7, 141.8, 134.9, 133.5, 132.9, 130.5, 129.8, 127.9, 127.8, 124.9, 124.6, 123.7, 122.2, 121.7, 120.2, 119.3, 117.4, 65.6, 20.7. FAB-MS: calcd. MW, 539.7, *m/e* = 539.3 (M<sup>+</sup>).

### Synthesis of 7-(diphenylamino)-9,9'-spirobifluorene-2-carboxaldehyde (PhSPCHO)

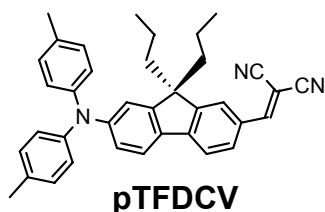


Under nitrogen atmosphere, a mixture of 7-bromo-9,9'-spirobifluorene-2-

carboxaldehyde (4.5 g, 10.6 mmol), diphenylamine (2.7 g, 15.9 mmol), Pd(OAc)<sub>2</sub> (0.060 g, 0.27 mmol, 2.5 mol%), P(<sup>t</sup>Bu)<sub>3</sub> (0.12 g, 0.55 mmol, 5 mol%), and Cs<sub>2</sub>CO<sub>3</sub> (5.19 g, 15.9 mmol) in toluene (22 mL) was heated at 90 °C with stirring overnight. After cooling to room temperature, saturated ammonium chloride solution was added to the reaction solution. The solution was extracted with ethyl acetate, dried over MgSO<sub>4</sub>. The solution was concentrated under reduced pressure and subjected to flash column chromatography (silica gel, ethyl acetate/hexanes: 1/10). A greenish yellow solid was obtained. Yield: 95% (5.2 g). <sup>1</sup>H NMR (400 MHz, CDCl<sub>3</sub>): δ [ppm] 9.76 (s, 1H), 7.85–7.78 (m, 2H), 7.76 (d, 2H, *J* = 7.6 Hz), 7.71 (d, 1H, *J* = 8.2 Hz), 7.33 (td, 2H, *J* = 7.5 Hz, 1.0 Hz), 7.15–7.08 (m, 7H), 7.01 (dd, 1H, *J* = 8.4 Hz, 2.2 Hz), 6.95–6.89 (m, 6H), 6.77 (d, 2H, *J* = 7.6 Hz), 6.54 (d, 1H, *J* = 2.0 Hz). <sup>13</sup>C NMR (100 MHz, CDCl<sub>3</sub>): δ [ppm] 191.6, 151.6, 149.6, 149.2, 147.8, 147.6, 147.2, 141.8, 135.1, 134.4, 130.5, 129.1, 128.0, 127.8, 125.0, 124.4, 123.7, 123.3, 123.2, 121.8, 120.3, 119.5, 118.7, 65.6. FAB-MS: calcd. MW, 511.6, *m/e* = 511.2 (M<sup>+</sup>).



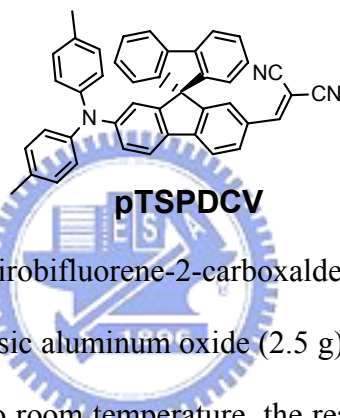
### Synthesis of 2-[7-(di-*p*-tolylamino)-9,9'-dipropyl-9H-fluoren-2-ylmethylene]malononitrile (pTFDCV)



7-(Di-*p*-tolylamino)-9,9'-dipropylfluorene-2-carboxaldehyde (2 g, 42.23 mmol), malononitrile (0.56 g, 8.45 mmol) and basic aluminum oxide (2 g) are stirred in toluene (20 mL) for 24 h at 100 °C. After cooling to room temperature, the reaction solution was filtered. The filtrate was subjected to flash column chromatography (silica gel, ethyl acetate/hexanes: 1/20). A red solid was obtained. Yield: 90% (2.0 g). <sup>1</sup>H NMR (400 MHz, CDCl<sub>3</sub>): δ [ppm] 7.85 (d, 1H, *J* = 1.4 Hz), 7.79 (dd, 1H, *J* = 8.1 Hz, 1.7 Hz), 7.78 (s, 1H), 7.63 (d, 1H, 8.1 Hz),

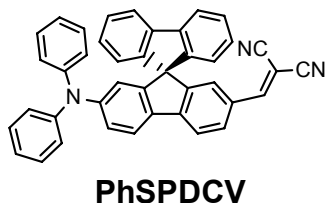
7.52 (d, 1H, 8.4 Hz), 7.08 (d, 4H, 8.5 Hz), 7.03–7.00 (m, 5H), 6.93 (dd, 1H,  $J = 8.4$  Hz, 2.1 Hz), 2.32 (s, 6H), 1.91–1.75 (m, 4H), 0.73–0.58 (m, 10H).  $^{13}\text{C}$  NMR (100 MHz,  $\text{CDCl}_3$ ):  $\delta$  [ppm] 159.7, 154.0, 151.6, 150.1, 148.5, 144.9, 133.4, 132.2, 131.4, 130.0, 128.5, 125.0, 124.5, 121.9, 121.1, 119.3, 116.0, 114.7, 113.6, 78.9, 55.4, 42.2, 20.8, 17.3, 14.4. FAB-MS: calcd. MW, 521.7,  $m/e = 521.3$  ( $\text{M}^+$ ). Anal. Found (calcd.) for  $\text{C}_{37}\text{H}_{35}\text{N}_3$ : C 85.32 (85.18), H 6.56 (6.76), N 7.97 (8.05).

### Synthesis of 2-[7-(di-*p*-tolylamino)-9,9'-spirobifluorene-2-ylmethylene]malononitrile (pTSPDCV)



7-(Di-*p*-tolylamino)-9,9'-spirobifluorene-2-carboxaldehyde (2.5 g, 4.63 mmol), malononitrile (0.63 g, 9.5 mmol), and basic aluminum oxide (2.5 g) are stirred in toluene (10 mL) for 24 h at 100 °C. After cooling to room temperature, the reaction solution was filtered. The filtrate was subjected to flash column chromatography (silica gel, ethyl acetate/hexanes: 1/20). A red solid was obtained. Yield: 76% (2.3 g).  $^1\text{H}$  NMR (400 MHz,  $\text{CDCl}_3$ ):  $\delta$  [ppm] 8.13 (dd, 1H,  $J = 8.2$  Hz, 1.4 Hz), 7.85–7.75 (m, 3H), 7.66 (d, 1H, 8.5 Hz), 7.47 (s, 1H), 7.35 (td, 2H,  $J = 7.5$  Hz, 1.1 Hz), 7.13 (td, 2H,  $J = 7.5$  Hz, 1.1 Hz), 6.94–6.90 (m, 5H), 6.90–6.82 (m, 5H), 6.76 (d, 2H, 7.3 Hz), 6.51 (s, 1H), 2.23 (s, 6H).  $^{13}\text{C}$  NMR (100 MHz,  $\text{CDCl}_3$ ):  $\delta$  [ppm] 159.2, 151.6, 150.3, 150.0, 148.4, 147.3, 144.4, 141.7, 133.3, 132.8, 129.8, 129.7, 129.0, 128.1, 127.9, 127.6, 124.8, 123.6, 122.1, 121.8, 120.3, 119.8, 116.7, 114.3, 113.2, 79.4, 65.6, 20.7. FAB-MS: calcd. MW, 587.7,  $m/e = 587.2$  ( $\text{M}^+$ ). Anal. Found (calcd.) for  $\text{C}_{43}\text{H}_{29}\text{N}_3$ : C 87.92(87.88), H 4.76(4.97), N 7.11 (7.15).

**Synthesis of 2-[7-(diphenylamino)-9,9'-spirobifluorene-2-ylmethylene]malononitrile (PhSPDCV)**

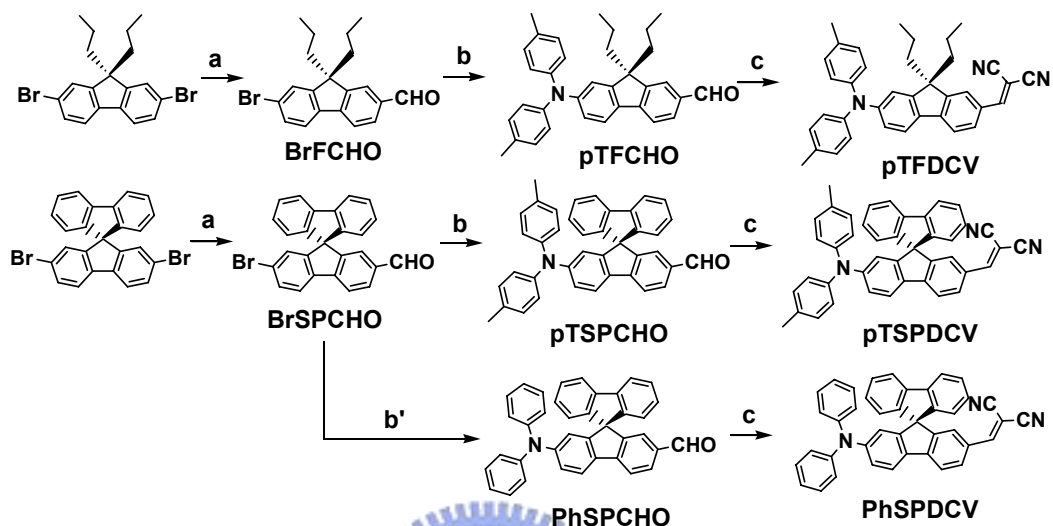


7-Diphenylamino-9,9'-spirobifluorene-2-carboxaldehyde (3.5 g, 6.84 mmol), malononitrile (1.4 g, 21.2 mmol), and basic aluminum oxide (3.5 g) are stirred in toluene (34 mL) for 24 h at 100 °C. After cooling to room temperature, the reaction solution was filtered. The filtrate was subjected to flash column chromatography (silica gel, ethyl acetate/hexanes: 1/20). A red solid was obtained. Yield: 73% (3.0g). <sup>1</sup>H NMR (400 MHz, CDCl<sub>3</sub>): δ [ppm] 8.15 (dd, 1H, *J* = 8.2 Hz, 1.8 Hz), 7.81 (d, 1H, *J* = 8.2 Hz), 7.76 (d, 2H, *J* = 7.6 Hz), 7.71 (d, 1H, *J* = 8.4 Hz), 7.43 (s, 1H), 7.35 (td, 2H, *J* = 7.5 Hz, 1.1 Hz), 7.15–7.09 (m, 6H), 7.00 (dd, 1H, *J* = 8.4 Hz, 2.2 Hz), 6.97–6.92 (m, 6H), 6.87 (d, 1H, *J* = 1.6 Hz), 6.76 (d, 2H, 7.6 Hz), 6.53 (d, 1H, *J* = 2.1 Hz). <sup>13</sup>C NMR (100 MHz, CDCl<sub>3</sub>): δ [ppm] 159.2, 151.7, 150.1, 149.9, 148.2, 147.1, 146.9, 141.7, 133.7, 129.6, 129.3, 129.2, 128.2, 127.9, 127.8, 124.7, 123.6, 123.5, 122.9, 122.2, 120.4, 120.1, 118.0, 114.2, 113.1, 79.7, 65.6. FAB-MS: calcd. MW, 559.7, *m/e* = 559.3 (M<sup>+</sup>). Anal. Found (calcd.) for C<sub>41</sub>H<sub>25</sub>N<sub>3</sub>: C 87.99 (87.94), H 4.50 (4.48), N 7.51 (7.60).

## 2-4 Results and Discussion

### 2-4-1 Synthesis

Scheme 2-1



Reagents and conditions: (a) *n*-BuLi, THF,  $-78\text{ }^{\circ}\text{C}$ , then DMF, RT, 3 h, 79% (**BrFCHO**), 75% (**BrSPCHO**); (b and b') di(*p*-tolyl)amine or diphenylamine,  $\text{Cs}_2\text{CO}_3$ , Pd(OAc) $_2$ , P(*t*Bu) $_3$ , toluene,  $120\text{ }^{\circ}\text{C}$ , 8 h, 86% (**pTFCHO**), 75% (**pTSPCHO**), 95% (**PhSPCHO**); (c) malononitrile, basic  $\text{Al}_2\text{O}_3$ , toluene,  $70\text{ }^{\circ}\text{C}$ , 16 h, 90% (**pTFDCV**), 76% (**pTSPDCV**), 73% (**PhSPDCV**).

The synthetic routes to three red emitting fluorene derivatives (**pTFDCV**, **pTSPDCV**, and **PhSPDCV**) are shown in Scheme 2-1. The syntheses are rather similar and straightforward. Either 2,7-dibromo-9,9'-dipropylfluorene or 2,7-dibromo-9,9'-spirobifluorene was lithiated with a stoichiometric amount of *n*-BuLi at  $-78\text{ }^{\circ}\text{C}$ , followed by the reaction with DMF and subsequent acidic hydrolysis. The following arylation of the aldehyde-carrying fluorene derivative, **BrFCHO** or **BrSPCHO**, was readily performed in the presence of palladium catalyst and a non-nucleophilic base,  $\text{Cs}_2\text{CO}_3$  being the most suitable. Finally, malononitrile was condensed under Knoevenagel conditions (basic  $\text{Al}_2\text{O}_3$  in dry toluene) with the aldehyde functionality to form the dicyanovinyl electron-withdrawing group of red emitting fluorene compounds. Three red emitting fluorenes isolated from

reactions were purified by column chromatography and further by train sublimation for the need of OLED fabrication. They were characterized by elemental analysis, mass spectrometry, and NMR spectroscopy, and were consistent with the proposed structures.

#### 2-4-2 Analysis of X-ray Crystal structure

**pTSPDCV** and **PhSPDCV** were examined for molecular packing in solid state by single crystal x-ray analysis.<sup>[25]</sup> The crystal structures of **pTSPDCV** and **PhSPDCV** (**Figure 2-15**) reveal the unique non-planar molecular structure and the loose packing nature of the material. Molecule wise, both fluorene parts of the spirobifluorene moieties are essentially planar as expected. While the dicyanovinyl acceptor is only slightly twisted (dihedral angle  $\sim 28^\circ$ ) from the coplanar conformation with the fluorene ring, the two 4-tolyl or phenyl rings are twisted in large angle ( $\sim 60^\circ$ ) to the planar fluorene ring causing a distinct bulge, in addition to the rigid and bulky spiro-annulation, of **pTSPDCV** or **PhSPDCV**. Both structural features of arylamino bulge and orthogonal spiro-annulation are essential in preventing **pTSPDCV** or **PhSPDCV** molecule from close packing and hence severe fluorescence quenching. The crystal of **pTSPDCV** or **PhSPDCV** is composed of antiparallel arrays of each molecule approximately along *b*-axis of the unit cell (**Figure 2-15**). Each head-to-tail aligned repeating fluorene molecule in the crystal of either **pTSPDCV** or **PhSPDCV** has an about 4~5 Å (about the half distance of the of *a*-axis) vertical displacement along the normal of the fluorene ring, which can be attributed to the intrusion of bulgy *p*-tolyl or phenyl moieties in crystal packing. Such 4~5 Å separation makes vertical plane-to-plane  $\pi$ - $\pi$  interaction between fluorene rings out of the reach in both crystals. In addition to several weak van der Waals non  $\pi$ - $\pi$  interactions,<sup>[26]</sup> the weak dipole-dipole interactions in long distance appear to be the major force in holding the crystal packing together and causing the fluorescence quenching.



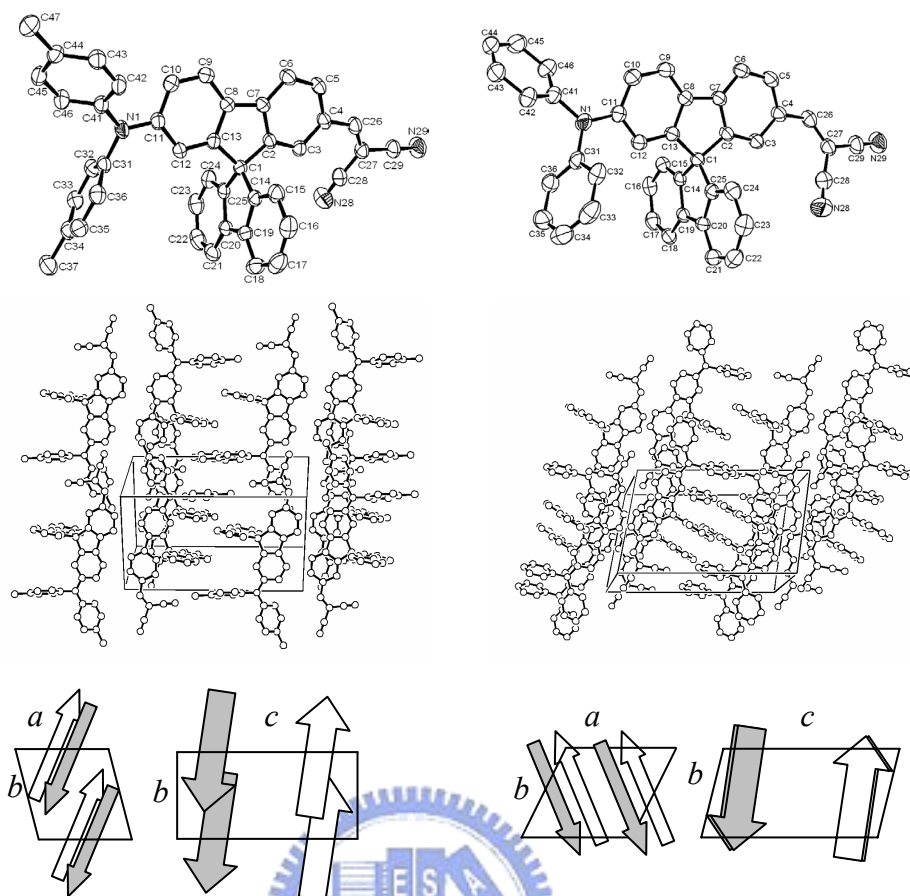


**Figure 2-15.** X-ray determined molecular structure and crystal packing diagram of **pTSPDCV** (left column) and **PhSPDCV** (right column). All of the hydrogen atoms are removed for clarity. The *b*-axis and *c*-axis are the vertical and the longest one, respectively. Sketches below each diagram depict the crystal packing in the unit cell of **pTSPDCV** (bottom left) and **PhSPDCV** (bottom right) viewing from *c*- and *a*-axis. The arrows indicate the direction from the arylamino to dicyanovinyl substituent.

### 2-4-3 Thermal Analysis

**Table 2-2.** Optical and thermal properties of red emitting fluorenes

	Solution				Solid Film		$T_m$ (°C)	$T_g$ (°C)	$T_c$ (°C)	$T_d$ (°C)
	$\lambda_{max}^{fl}$ (nm) <sup>a</sup>	$\lambda_{max}^{fl}$ (nm) <sup>b</sup>	$\lambda_{max}^{fl}$ (nm) <sup>c</sup>	$\Phi_f$ (%) <sup>d</sup>	$\lambda_{max}^{fl}$ (nm)	$\Phi_f$ (%)				
<b>pTFDCV</b>	516	596	652	74	657	27	223	e	179	298
<b>pTSPDCV</b>	516	598	658	75	665	25	232 <sup>f</sup>	122	e	340
<b>PhSPDCV</b>	500	572	624	70	633	33	253 <sup>f</sup>	110	e	337
Nile Red	527	576	596	67	e	~0				
DCM	501	549	564	8	665	5				

<sup>a</sup>In hexanes. <sup>b</sup>In 1,4-dioxane. <sup>c</sup>In chloroform. <sup>d</sup>In 1,4-dioxane. <sup>e</sup>Not observed. <sup>f</sup>Only observed for the sample in the first heating scan.

Thermal analysis of three red emitting fluorene derivatives indicated that spiro-bifluorenes **pTSPDCV** and **PhSPDCV** have a better-desired thermal property than **pTFDCV**. This is evident in the repeated heating and cooling scans of DSC. All sublimed samples of three red emitting fluorene derivatives were detected for a distinct melting temperature ( $T_m$ ) above 220 °C in the first heating scan (**Table 2-2**). However, for the rest of heating scans, the  $T_m$  signal no longer existed and **pTSPDCV** and **PhSPDCV** exhibited only step-like weak endothermic signals at 122 and 110 °C, respectively, (**Table 2-2**) indicative of  $T_g$ . Conversely, the heating scans of **pTFDCV** were detected for only  $T_m$  at 223 °C but no  $T_g$  signal, indicative of crystalline nature of **pTFDCV**. For the cooling scans of DSC, **pTSPDCV** and **PhSPDCV** showed only  $T_g$  and no exothermic signal of crystallization temperature ( $T_c$ ), which is in sharp contrast to **pTFDCV** showing only  $T_c$  at ~179 °C instead of  $T_g$  signal. The thermal analysis of DSC clearly demonstrated that the spiro-annulated bifluorene is a potent structure moiety useful for red emitting fluorene fluorophores in inhibiting the crystallization in solid state. Spiro-annulated bifluorenes (**pTSPDCV** and **PhSPDCV**) also exhibited the advantage of thermal stability. They showed thermal decomposition temperatures ( $T_{ds}$ ) about 40 °C higher than **pTFDCV** (**Table 2-2**).



**Figure 2-16.** White light (top) and UV (bottom) illumination of the powder of Nile Red, DCM, **pTFDCV**, **pTSPDCV**, and **PhSPDCV** (from left to right), respectively.

#### 2-3-4 Fluorescence Analysis

All **pTFDCV**, **pTSPDCV**, and **PhSPDCV** emit green (in hexanes), or yellow-orange (in 1,4-dioxane) to red (in chloroform or acetonitrile) fluorescence in solution highly depending

on the solvent polarity (**Table 2-2**). This solvatochromic behavior is consistent with the charge-transfer (CT) characteristic of the donor-acceptor substituted red emitting fluorenes, and it is similar to that of Nile Red and DCM. However, in solid state, all three fluorene derivatives show red fluorescence with  $\lambda_{\max}^{\text{fl}} > 640$  nm (see **Table 2-2**), satisfying the requirement for red OLEDs. In solution (1,4-dioxane), these red fluorophores exhibit intense fluorescence (solution fluorescence quantum yield  $\Phi_f$  is 70~75%), comparable with classical red fluorophore Nile Red ( $\Phi_f$  is 67%) but much stronger than red laser dye DCM ( $\Phi_f$  is 8%). Conversely, they are all much brighter red fluorophores compared with the dull Nile Red or DCM in solid state (see fluorescence images shown in **Figure 2-15**). The measurement of semi-crystalline solid films indicated the solid film fluorescence quantum yields of three red emitting fluorene derivatives are in the range of 25-33% (**Table 2-2**), which are far more higher than ~0% and 5% of Nile Red and DCM, respectively. This should be attributed to the anti-aggregation molecular design of the red emitting fluorenes. Therefore, unlike the red dopant of Nile Red or DCM, **pTFDCV**, **pTSPDCV**, and **PhSPDCV** are all suitable as the red host emitters in the fabrication of non-doped red OLEDs.

#### 2-4-5 Characterization of red OLEDs

**Table 2-3.** Characteristics of OLEDs containing **pTFDCV**, **pTSPDCV**, and **PhSPDCV**.

Devices <sup>a</sup>	Max. Luminance (cd/m <sup>2</sup> )	Luminance, Efficiency, Voltage (cd/m <sup>2</sup> , %, V) <sup>b</sup>	Max. Efficiency (%), (cd/A, lm/W)	$\lambda_{\max}^{\text{el}}$ (nm)	CIE 1931 Chromaticity (x, y)
I	6570	359, 2.0, 7.5	2.1, 1.8, 0.8	644	0.65, 0.35
II	6080	301, 2.3, 7.7	2.6, 1.8, 0.9	652	0.66, 0.33
III	11380	615, 3.2, 8.1	3.6, 3.5, 1.8	638	0.65, 0.35
IV	12410	557, 2.9, 7.3	3.0, 2.9, 1.4	636	0.65, 0.35
V	10640	622, 3.2, 7.9	3.5, 3.4, 1.6	636	0.65, 0.35

<sup>a</sup>Device I: ITO/NPB(10 nm)/**pTFDCV** (40nm)/BCP (20nm)/Alq<sub>3</sub>(30 nm)/Mg:Ag; Device II: ITO/NPB(10 nm)/**pTSPDCV** (40nm)/BCP (20nm)/Alq<sub>3</sub>(30 nm)/Mg:Ag; Device III: ITO/NPB(10 nm)/**PhSPDCV** (40nm)/BCP (20nm)/Alq<sub>3</sub>(30 nm)/Mg:Ag; Device IV: ITO/NPB(5 nm)/**PhSPDCV** (40nm)/BCP (10nm)/Alq<sub>3</sub>(30 nm)/Mg:Ag; Device V: ITO/NPB(10 nm)/**PhSPDCV** (50nm)/BCP (15nm)/Alq<sub>3</sub>(30 nm)/Mg:Ag; <sup>b</sup>At current density of 20 mA/cm<sup>2</sup>

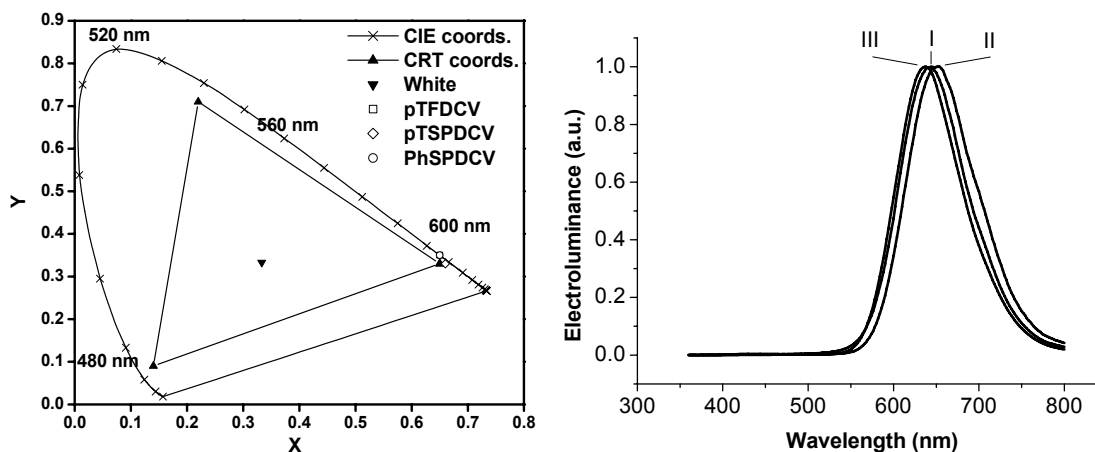


**Figure 2-17.** CIE 1931 chromaticity diagram (left) and EL spectra (right) of device I, II, and III containing **pTFDCV**, **pTSPDCV**, and **PhSPDCV**, respectively.

**pTFDCV**, **pTSPDCV** and **PhSPDCV** were each adopted in the fabrication of non-doped, host-emitting, red OLEDs of devices I-III (**Table 2-3**) with the same configuration for comparison purpose. Authentic red EL was observed for these devices (**Table 2-3** and **Figure 2-16**). Device III has the shortest EL wavelength among three devices reflected to the shortest PL wavelength among three red emitting fluorenes. Regardless the difference of  $\lambda_{\max}^{\text{el}}$ , they are all sufficiently red and have comparable chromaticity as CRT (Cathode Ray Tube) Phosphors either American or European standard red color according to 1931 CIE (Commission Internationale de l'Eclairage) chromaticity diagram ( $x = 0.63\text{-}0.64$ ,  $y = 0.33\text{-}0.34$ ).<sup>[27]</sup> Each device can be turned on between 3 and 5 V and showing red EL with the intensity in the range of 300-615  $\text{cd}/\text{m}^2$  at low current density of 20  $\text{mA}/\text{cm}^2$  (about 7-8 V), which is sufficient bright and practical for the flat panel display application. Device III shows the highest electroluminescence of 11400  $\text{cd}/\text{m}^2$  and external quantum efficiency of 3.6% among the three devices, which is quite consistent with the higher fluorescence quantum yield of **PhSPDCV** than those of **pTFDCV** and **pTSPDCV** in solid state (**Table 2-2**). The performances of the red OLEDs can be further enhanced by the adjustment of the layer thickness, such as the narrowing of the hole-transporting layer (NPB) and hole-blocking layer (BCP) as those in devices IV. The maximum luminance can be boosted over 12000  $\text{cd}/\text{m}^2$  in

device IV with the same red chromaticity but in sacrifice of some efficiency. The lost efficiency can be mostly recovered by the widening the host-emitting layer (**PhSPDCV**) as well as the hole-blocking layer (BCP) shown in device V. It is noteworthy that the devices I-V all show reasonable stable efficiency with only modest decay in the low current density range of 1-20 mA/cm<sup>2</sup> (**Figure 2-18**), which is a satisfactory performance matching the need for active-matrix-driven devices. Particularly, device V exhibited relatively stable  $\eta_{\text{EXT}}$  (decrease from 3.5 to 3.3%) in the current density up to 15 mA/cm<sup>2</sup>. This is the first demonstration that the stable efficiency can be achieved for host-emitting, non-doped, red OLEDs, which usually show sharp decay of EL efficiency even at medium range of current density or driving voltage. It seems that the stability of device EL efficiency can be adjusted by the thickness of hole-transporting NPB or hole-blocking BCP in conjunction with the red light-emitting layers. Nevertheless, to our best knowledge, these devices exhibit some of the very best performances observed for fluorophore-based red OLEDs, either dopant or non-doped devices.



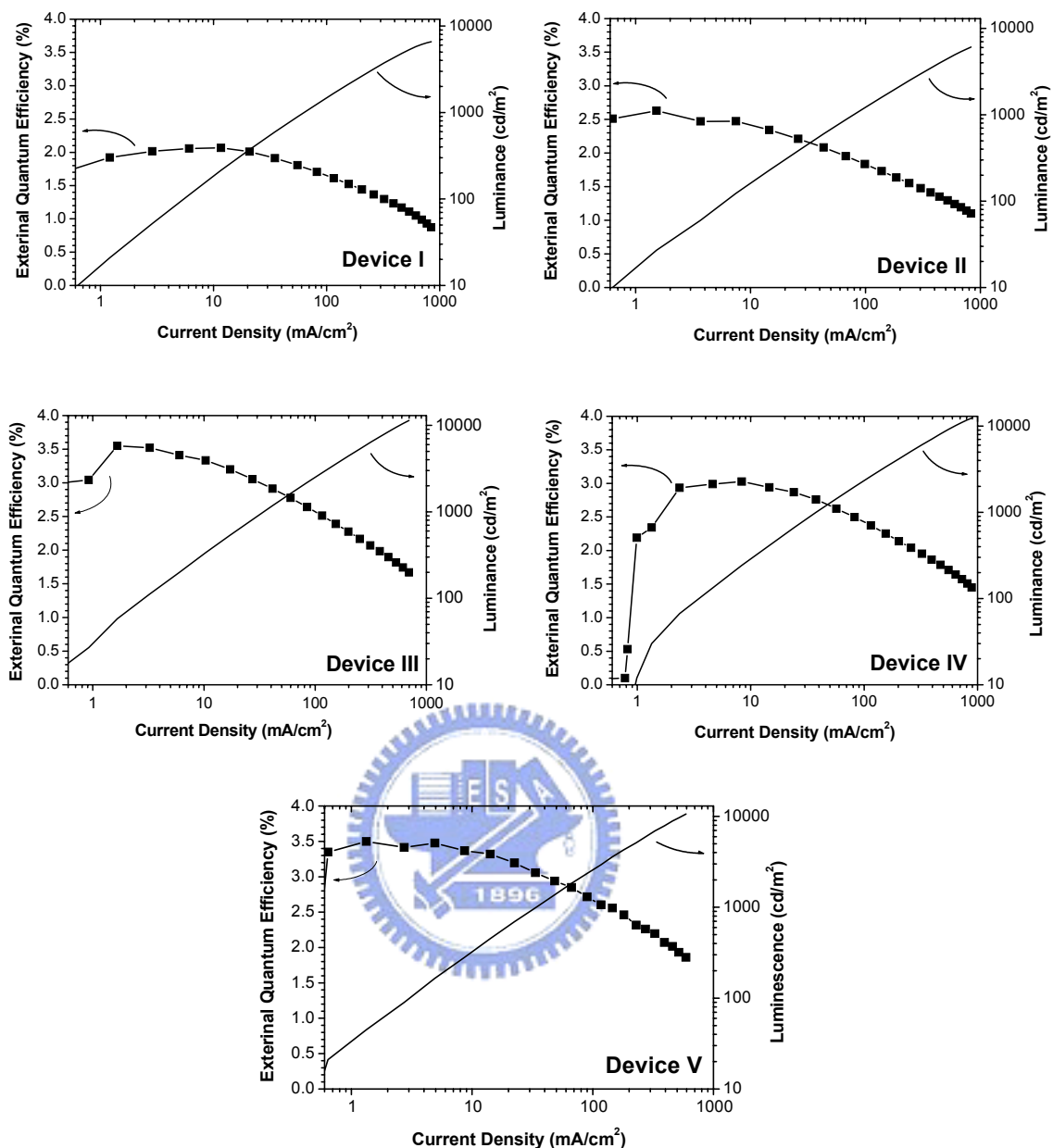


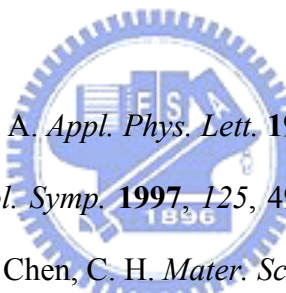
**Figure 2-18.** External quantum efficiency-Current density-EL intensity ( $\eta_{\text{EXT}}-I-L$ ) characteristics of devices I-V.

## 2-5 Conclusion

In summary, we have successfully designed and synthesized fluorene derivatives capable of emitting red fluorescence. The nonplanar arylamino group and the rigid spiro-annulation can effectively overcome the aggregation and hence the fluorescence quenching in solid state. We justified our approach with several physical characterizations, including crystal x-ray structure, DSC analysis, and fluorescence quantum yield. The high performance of

non-doped red OLEDs fabricated with the host-emitting red emitting fluorene materials further verifies our purpose. Application wise, with the material of newly designed fluorene compounds, the troublesome dopant process in the fabrication of red OLEDs is evitable, which is good news for commercial mass production process. We have demonstrated that the performance of fluorene-based non-doped red OLEDs is the best so far and comes close to the best of dopant-based red OLEDs (DCJTb as the red dopant having 4.4 cd/A maximum efficiency and brightness 966 cd/m<sup>2</sup> at 20 mA/cm<sup>2</sup>).<sup>[28]</sup> In the context of developing effective fluorene-based fluorophores in solid state, the same molecular design principle can be applied to fluorenes emitting light other than red color. This is currently under active investigation.

## 2-6 References

- 
- [1] Tang, C. W.; VanSlyke, S. A. *Appl. Phys. Lett.* **1987**, *51*, 913.
  - [2] (a) Hsieh, B. R. *Macromol. Symp.* **1997**, *125*, 49.; (b) Chen, C.-T. *Chem. Mater.* **2004**, *16*, 4389.; (c) Hung, L. S.; Chen, C. H. *Mater. Sci. Eng.* **2002**, *R39*, 143.
  - [3] (a) Burrows, P. E.; Forrest, S. R.; Silbey, S. P.; Thompson, M. E. *Appl. Phys. Lett.* **1996**, *69*, 2959.; (b) Shen, Z.; Burrows, P. E.; Bulovic, V.; Forrest, S. R.; Thompson, M. E. *Science* **1997**, *276*, 2009.
  - [4] Sarkar, N.; Das, K.; Narayan, D.; Bhattachartha, K. *Langmuir* **1994**, *10*, 326.
  - [5] Tang, C. W.; VanSlyke, S. A.; Chen, C. H. *J. Appl. Phys.* **1989**, *65*, 3610.
  - [6] Toguchi, S.; Morioka, Y.; Ishikawa, H.; Oda, A.; Hasegawa, E. *Synth. Met.* **2000**, *111-112*, 57.
  - [7] Huang, T.-H.; Lin, J. T.; Tao, Y. T.; Chuen, C.-H. *Chem. Mater.* **2003**, *15*, 4584.
  - [8] Kim, D. U.; Paik, S. H.; Kim, S.-H.; Tsutsui, T. *Synth. Met.* **2001**, *123*, 43.
  - [9] Thomas, K. R. J.; Lin, J. T.; Velusamy, M.; Tao, Y.-T.; Chuen, C.-H. *Adv. Funct. Mater.* **2004**, *14*, 83.

- [10] Yeh, H.-C.; Yeh, S.-J.; Chen, C.-T. *Chem. Commun.* **2003**, 2632.
- [11] Thomas, K. R. J.; Lin, J. T.; Tao, Y.-T.; Chuen, C.-H. *Adv. Mater.* **2002**, *14*, 822.
- [12] Chen, S.; Xu, X.; Liu, Y.; Yu, G.; Sun, X.; Qiu, W.; Ma, Y.; Zhu, D. *Adv. Funct. Mater.* **2005**, *15*, 1541.
- [13] Chen, C.-T.; Lin, J.-S.; Moturu, M. V. R. K.; Chao, W.-S.; Tao, Y.-T.; Chien, C.-H. *J. Am. Chem. Soc.* **2006**, *128*, 10992.
- [14] Wu, W.-C.; Yeh, H.-C.; Chan, L.-H.; Chen, C.-T. *Adv. Mater.* **2002**, *14*, 1072.
- [15] Chiu, C.-W.; Chow, T. J.; Chuen, C.-H.; Lin, H.-Me.; Tao, Y.-T. *Chem. Mater.* **2003**, *15*, 4527.
- [16] (a) Reinhardt, B. A.; Brott, L. L.; Clarson, S. J.; Dillard, A. G.; Bhatt, J. C.; Kannan, R.; Yuan, L.; He, G. S.; Prasad, P. N. *Chem. Mater.* **1998**, *10*, 1863.; (b) Belfield, K. D.; Hagan, D. J.; Van Stryland, E. W.; Schafer, K. J.; Negres, R. A. *Org. Lett.* **1999**, *1*, 1575.; (c) Belfield, K. D.; Schafer, K. J.; Mourad, W.; Reinhardt, B. A. *J. Org. Chem.* **2000**, *65*, 4475. (d) Kannan, R.; He, G. S.; Yuan, L.; Xu, F.; Prasad, P. N.; Dombroskie, A. G.; Reinhardt, B. A.; Bauer, J. W.; Vaia, R. A.; Tan, L.-S. *Chem. Mater.* **2001**, *13*, 1896.; (e) Pudzich, R.; Salbeck, J. *Synth. Met.* **2003**, *138*, 21.
- [17] (a) Salbeck, J.; Yu, N.; Bauer, J.; Weissörtel, F.; Bestgen, B. *Synth. Met.* **1997**, *91*, 209.; (b) Salbeck, J.; Weissörtel, F.; Bauer, J. *Macromol. Symp.* **1997**, *125*, 121.; (c) Steuber, F.; Staudigel, J.; Stössel, M.; Simmerer, J.; Winnacker, A.; Spreitzer, H.; Weissörtel, F.; Salbeck, J. *Adv. Mater.* **2000**, *12*, 130.
- [18] (a) Konne, B. E.; Loy, D. E.; Thompson, M. E. *Chem. Mater.* **1998**, *10*, 2235.; (b) Shirota, Y. *J. Mater. Chem.* **2000**, *10*, 1.; (c) Strohriegl, P.; Grazulevicius, J. V. *Adv. Mater.* **2002**, *14*, 1439.; (d) Thelakkat, M.; *Macromol. Mater. Eng.* **2002**, *287*, 442. (e) Chen, C.-T.; Chiang, C.-L.; Lin, Y.-T.; Chan, L.-H.; Huang, C.-H.; Tsai, Z.-W.; Chen, C.-T. *Org. Lett.* **2003**, *6*, 1261.



- [19] (a) Brütting, W.; Berleb, S.; Egerer, G.; Schwoerer, M.; Wehrmann, R.; Elschner, A. *Synth. Met.* **1997**, *91*, 325.; (b) Berleb, S.; Schwoerer, M.; Wehrmann, R.; Elschner, A. *J. Appl. Phys.* **1998**, *83*, 4403.
- [20] Kelley, C. J.; Ghiorghis, A. J.; Kauffman, M. *J. Chem. Res. (M)* **1997**, 2701.
- [21] Lupo, D.; Salbeck, J.; Schenk, H.; Stehlin, T.; Stern, R.; Wolf, A. US Patent 5840217, **1998**.
- [22] Sheldrick, G. M. *SHELXL-97*, University of Göttingen, Germany, **1997**.
- [23] Farrugia, L. J. *J. Appl. Cryst.* **1999**, *32*, 837.
- [24] Chan, L.-H.; Lee, R.-H.; Hsieh, C.-F.; Yeh, H.-C.; Chen, C.-T. *J. Am. Chem. Soc.* **2002**, *124*, 6469.
- [25] Crystal data for **pTSPDCV**:  $C_{43}H_{29}N_3$ ;  $F_w = 587.69$ , triclinic,  $P-1$ ,  $Z = 2$ ,  $F(000) = 616$ . Cell dimensions:  $a = 9.01271(2) \text{ \AA}$ ;  $b = 10.4903(2) \text{ \AA}$ ;  $c = 17.0098(4) \text{ \AA}$ ;  $\alpha = 88.9890(10)^\circ$ ;  $\beta = 84.8000(10)^\circ$ ;  $\gamma = 82.4450(10)^\circ$ .  $V = 1590.20(6) \text{ \AA}^3$ ,  $2\theta_{\max} = 50.0^\circ$ ,  $\rho_{\text{calcd}} = 1.227 \text{ g cm}^{-3}$ . Of 7837 reflections, 5575 were independent, 416 parameters,  $R(F_o) = 0.0675$  (for reflections with  $I > 2\sigma(I)$ ),  $R_w(F_o) = 0.1659$  (for reflections with  $I > 2\sigma(I)$ ). The GoF on  $F^2$  was equal 0.950. Crystal data for **PhSPDCV**:  $C_{41}H_{25}N_3$ ;  $F_w = 559.64$ , triclinic,  $P-1$ ,  $Z = 2$ ,  $F(000) = 584$ . Cell dimensions:  $a = 8.8833(9) \text{ \AA}$ ;  $b = 10.6370(16) \text{ \AA}$ ;  $c = 16.457(4) \text{ \AA}$ ;  $\alpha = 100.104(16)^\circ$ ;  $\beta = 97.420(14)^\circ$ ;  $\gamma = 97.564(11)^\circ$ .  $V = 14990.0(4) \text{ \AA}^3$ ,  $2\theta_{\max} = 50.0^\circ$ ,  $\rho_{\text{calcd}} = 1.240 \text{ g cm}^{-3}$ . Of 5637 reflections, 5263 were independent, 416 parameters,  $R(F_o) = 0.0378$  (for reflections with  $I > 2\sigma(I)$ ),  $R_w(F_o) = 0.1054$  (for reflections with  $I > 2\sigma(I)$ ). The GoF on  $F^2$  was equal 0.988. CCDC 225757 and CCDC 225758 contain the supplementary crystallographic data of **pTSPDCV** and **PhSPDCV**, respectively. These data can be obtained free of charge via [www.ccd.cam.ac.uk/conts/retrieving.html](http://www.ccd.cam.ac.uk/conts/retrieving.html) (or from the Cambridge Crystallographic Data Centre, 12, Union Road, Cambridge CB21EZ, UK; fax: (+44)1223-336-033; or [deposit@ccdc.cam.ac.uk](mailto:deposit@ccdc.cam.ac.uk)).

[26] The closest van der Waals contact (3.51 Å) of the crystal of **pTSPDCV** is observed for the hydrogen atoms of the methyl group of tolyl ring and the C(4) carbon of the fluorene moiety in the next unit cell. For the crystal of **PhSPDCV**, the horizontal edge-to-edge contact (3.35 Å) of phenyl ring and the spiro-annulated fluorene ring of the opposite molecular array in the central region of the unit cell is the closest one. The center region of both crystals is composed of a pair ladder-like structure, which is formed alternatively by the annulated 9,9'-biphenyl rings and 4-tolyl group of **pTSPDCV** or phenyl group of **PhSPDCV**. However, these aromatic rings are not parallel to each other and they are not even stacked straight-up preventing any substantial vertical  $\pi$ - $\pi$  interaction.

[27] Copper, A. D.; Cok, R. S.; Feldman, R. D. *SPIE-Int. Soc. Opt. Eng.* **2001**, 4105, 18.

[28] Liu, T.-H.; Iou, C.-Y.; Chen, C. H. *Appl. Phys. Lett.* **2003**, 83, 5241.

